

Gold alignment & internal dissipation

A. Lazarian¹

Astronomy Department, University of Texas, Austin, TX 78712-1083

ABSTRACT

The measures of mechanical alignment were obtained for both prolate and oblate grains when their temperature is comparable with grain kinetic energy divided by k , the Boltzmann constant. For such grains, the alignment of angular momentum, \mathbf{J} , with the axis of maximal inertia, \mathbf{a} , is only partial. This substantially alters the alignment as compared with the results in Lazarian (1995) and Roberge, Hanany & Messinger (1996) obtained on the assumption of perfect alignment. We also describe the Gold alignment when the Barnett dissipation is suppressed and derive an analytical expression which relates the measure of alignment with parameters of grain nonsphericity and the direction of the gas - grain drift. This solution provides the lower limit for the alignment measure, while the upper limit is given by the analytics derived in Lazarian (1994). Using results of a recent study of incomplete internal relaxation in Lazarian & Roberge (1996), we find measures of alignment for the whole range of ratios of grain rotational energy to k over T_s , where T_s is the grain temperature. To describe alignment for mildly supersonic drifts, we suggest an analytical approach which provides good correspondence with the results of direct numerical simulations in Roberge, Hanany & Messinger (1995). We also extend our approach to account for the simultaneous action of the Gold and Davis-Greenstein mechanisms.

Subject headings: dust, extinction — ISM, clouds — ISM, polarization

1. Introduction

Understanding the observed alignment of the ISM grains is yet unsolved astrophysical problem (see Hildebrand 1988, Whittet 1992, Goodman et al. 1995, Roberge 1996). This limits the use of polarimetry data for studying interstellar magnetic fields.

¹Present address: Department of Astrophysical Sciences, Princeton University, Princeton, NJ 08544

The mechanism of mechanical alignment of thermally rotating grains was pioneered by Gold (1951) the same year that the classical paper introducing the paramagnetic alignment by Davis & Greenstein (1951) was published. Originally, Gold suggested that grain alignment arises from cloud - cloud collisions (Gold 1951, 1952), but it was shown in Davis (1955), that such collisions can align only an insignificant fraction of interstellar grains. Therefore a further study of the mechanism was devoted mainly to the alignment in the vicinity of bright sources, where radiation pressure can drive grains to supersonic velocities (see Purcell 1969, Aitken et al. 1995). A new important idea, put forward by Roberge & Hanany (1990), that grains can be aligned by ambipolar diffusion made the Gold alignment more promising (see also Roberge, Hanany & Messinger 1995 hereafter RHM). Our study in Lazarian (1994, henceforth Paper I, and 1995a) showed that the role of mechanical processes had been underestimated. It was found that pervasive MHD waves² can produce grain alignment even within ideal MHD.

The goal of this paper is to provide an analytical quantitative description of the mechanical alignment of thermally rotating grains, referred to as “Gold alignment”. We distinguish between the Gold and mechanical alignment of suprathermally rotating grains (see Lazarian 1995a,b, Lazarian & Efrimsky 1996, Lazarian, Efrimsky & Ozik 1996).

Although the expressions for the measure of alignment corresponding to Gold alignment were obtained in Paper I, the shortcoming of this study was that only perfect alignment of angular momentum, \mathbf{J} , with the the principal axis of the maximal moment of inertia, \mathbf{a} , (henceforth the axis of major inertia) was considered. Although this regime is valid for highly supersonic motions discussed in Lazarian (Paper I), the wealth of the ISM conditions presents us with a wide range of other options.

It is well known from theoretical mechanics, that internal dissipation of energy cannot change grain angular momentum and, for a grain with fixed angular momentum, the minimal energy corresponds to rotation about the axis of major inertia. For suprathermally rotating grains, efficient internal dissipation of energy leading to nearly perfect alignment of angular momentum with the grain axis of major inertia was discovered by Purcell (1979) (see also Spitzer & McGlynn 1979). For thermally rotating grains, the alignment is only partial (Paper I, Lazarian & Roberge 1997, henceforth LR97).

To relate polarimetry observations, that are influenced by the alignment of the long grain axis, and the theory, that deals with the alignment of angular momentum, \mathbf{J} , one

²Here and further on in the paper when speaking about MHD waves we mean both Alfvénic and magnetosonic waves.

has to describe the alignment of \mathbf{J} not only in respect to magnetic field³, but also in respect to grain axes. These can be called external and internal alignment, respectively. Internal alignment arises both from the difference in grain moments of inertia (“Maxwellian alignment”) and due to the Barnett relaxation⁴ (“Barnett alignment”).

Below we use the statistical approach introduced in LR97. The gist of it is to describe deviations of \mathbf{J} from the axis of major inertia, \mathbf{a} , as thermal fluctuations from the position of static equilibrium when the time of internal relaxation is much shorter than that of the gaseous damping. By introducing the grain rotational temperature, which depends on both the temperature of the ambient gas and on the drift velocity, we show that, when the ratio of this temperature to the temperature of grain material tends to infinity, \mathbf{J} is coupled with \mathbf{a} , and this justifies our approach in Paper I. For finite ratios however, the deviations of \mathbf{J} become important for the alignment.

To describe Gold alignment for mildly supersonic velocities, we have to account for the rms motions of gas atoms. To do this, we assume that grains are subjected to a superposition of fluxes within a small angle to the direction of the initial flux and the value of this angle depends on the ratio of the flux velocity to the mean velocity of thermal motions. This enables us to obtain an asymptotic solution which provides fair agreement with the numerical calculations in RHM for the case of perfect coupling between \mathbf{J} and \mathbf{a} . Within the same model of perfect coupling the agreement with numerics in RHM is obtained for the joint action of Gold and Davis-Greenstein mechanisms. A comparison between numerics and analytics for the general case of incomplete internal alignment is planned, and we anxiously follow the progress of numerics in this direction.

The structure of the paper is as follows. First of all, we remind our reader of the concept of internal relaxation and describe how grain drift influences internal alignment (Sect. 2). Then in Sect. 3, we obtain analytical solutions for the alignment measure when internal relaxation is negligible and compare these results with the other extreme case, namely, when \mathbf{J} is perfectly coupled with \mathbf{a} . The treatment of the problem for an arbitrary degree of internal alignment is given in Sect. 4. In Sect. 5, we compare our results with numerics and argue that our analytical approach provides an adequate description of the alignment both for mildly supersonic velocities and for Gold and Davis-Greenstein processes

³Magnetic field acts as the axis of alignment because the time-scale of Larmor precession is usually much shorter than the time-scale of alignment. We remind the reader that the rapid Larmor precession arises from magnetic moments of grains; those moments are caused by the Barnett effect (Dolginov & Mytrophanov 1976).

⁴As a rule, the Barnett relaxation dominates internal relaxation (see Purcell 1979).

acting together. A short summary of results is presented in Sect. 6.

2. Internal alignment

As pointed out above, to relate theory and observations it is essential to describe the alignment of grain long axes in respect to magnetic field⁵. This alignment is determined uniquely by the alignment of grain angular momentum only if the angular momentum is coupled with the axis of major inertia, \mathbf{a} . Further we study a general problem when the internal alignment is partial.

Theoretical studies deal with the measure of alignment of angular momentum \mathbf{J} ⁶

$$Q_J = \frac{3}{2} \langle \cos^2 \theta_1 - \frac{1}{3} \rangle \quad , \quad (1)$$

where θ_1 is the angle between \mathbf{J} and the direction of magnetic field, while polarimetry provides us with the data on the Rayleigh reduction factor (Greenberg 1968)

$$R = \frac{3}{2} \langle \cos^2 \hat{\theta} \rangle - \frac{1}{2} \quad , \quad (2)$$

where $\hat{\theta}$ is the angle between the direction of magnetic field and the symmetry axis of a spheroid approximating the grain. The question how to relate these two quantities was on the astrophysical agenda from the very beginning of research in the area. First in Jones & Spitzer (1967), it was assumed that the distribution function of \mathbf{J} in the grain reference frame is independent of the alignment of \mathbf{J} in respect to magnetic field. This was a natural assumption to start with. Later, Spitzer (1978) showed that additional alignment of \mathbf{J} in respect to the axis of major inertia should be present due to paramagnetic relaxation in the external magnetic field. This effect can be called Spitzer relaxation to distinguish it from the Barnett relaxation discovered by Purcell (1979).

Here we assume that the ratio of the gas damping time to the time of internal relaxation is much greater than unity (see estimates in Roberge, DeGraff & Flaherty

⁵In a special case, e.g. in the atmospheres of comets, the alignment can happen on the time-scale less than that of precession. In such situations, the alignment should be defined in respect to the flow, which is similar to the alignment when the flow is directed along magnetic field and therefore we do not discuss it separately.

⁶Our notations are different from the ones used in Paper I. In an attempt to insure that the system of notations used by different authors is universal we adopt the system of notations suggested in review by Roberge (1996).

1993). In this case, the deviations of \mathbf{J} from the axis of major inertia, \mathbf{a} can be described thermodynamically (LR97).

For a grain with fixed angular momentum $J \equiv |\mathbf{J}|$ and with components of the moment of inertia related as $I_x < I_y < I_z$, the kinetic energy is

$$E = \frac{J^2}{2} \left[(1/I_x - 1/I_y) \sin^2 \xi \sin^2 \theta + (1/I_y - 1/I_z) \sin^2 \theta + 1/I_z \right] \quad , \quad (3)$$

where ξ is the azimuthal angle in the $x - y$ plane, and θ is the angle between \mathbf{J} and z -axis. Although the equilibrium position of the grain with fixed J^2 corresponds to $\theta \equiv 0$, thermal fluctuations cause deviations from it. These deviations can be described by the Boltzmann factor $\exp\{-E/(kT_s)\}$ (LR97).

A complex precession of \mathbf{J} due to these fluctuations modifies both the grain interaction with the gaseous flow and the dichroic absorption. However, it seems reasonable to assume that the behaviour of such an asymmetric grain can be approximated by the behaviour of a spheroidal grain with the moment of inertia somewhere between I_x and I_y (further on we denote this mean moment by I_\perp). Here we also adopt this approximation and hope to compare the results for spheroidal and irregular grains elsewhere.

For a spheroidal grain with temperature T_s , Eq. (3) can be simplified, and the distribution function of the angular momentum in the grain reference frame is (LR97)

$$f_{\text{TE}}(\theta_2) = \text{const} \times \sin \theta_2 \exp \left[-\frac{J^2}{2I_z k T_s} \left\{ (h - 1) \sin^2 \theta_2 + 1 \right\} \right] \quad , \quad (4)$$

where θ_2 is the angle between \mathbf{J} and the rotational symmetry axis of the spheroid, $h = I_z/I_\perp$ and the value of J is different for different grains of the ensemble. The fact that the probability of a particular angular momentum depends on angle θ_2 complicates the study. However, computations in LR97 show that with a sufficient degree of accuracy it is possible to substitute the rms value of J for a Maxwellian angular momentum distribution in Eq. (4) to get an approximate measure of alignment for an ensemble of grains with given rotational temperature. Therefore as the zero approximation we use

$$J^2 = kT_{\text{eff}} I_z (2/h + 1) \quad , \quad (5)$$

(Landau & Lifshitz 1980), where

$$T_{\text{eff}} \approx \frac{T_g + T_s}{2} + \frac{1}{3} \frac{mu^2}{2k} \quad , \quad (6)$$

m and u are the mass and velocity of bombarding atoms, respectively, and T_g is the gas temperature. We expect that numerical simulations by Roberge will determine the accuracy of the approximation adopted.

For hypersonic drifts in diffuse medium discussed in Paper I, $T_{\text{eff}} \gg T_s$ and the alignment of \mathbf{J} in the grain reference frame is close to being perfect. Indeed, if the drift velocity of grains exceeds the velocity of atoms in diffuse clouds 3 times, $T_s/T_{\text{eff}} \approx 0.1$. The corresponding distribution of \mathbf{J} (see Eq. (4)) has a peak near the axis of major inertia (see Fig. 1) and can be approximated by a delta-function. This, however, may not be true for a different grain environment. For instance in molecular clouds, gas and grains have similar temperatures and, for mildly supersonic drift velocities, T_{eff} is of the same order as T_s .

In short, perfect alignment between \mathbf{J} and \mathbf{a} does not seem to be universally applicable to interstellar grains. Below we describe the Gold alignment when this constraint is lifted.

3. Gold alignment for \mathbf{J} not parallel to \mathbf{a}

3.1. Analytics for the Rayleigh reduction factor in the absence of internal relaxation

The distribution of angular momentum can be characterized by function $f(n, \mathbf{J})$, where n is the number of grain-atomic collisions. In general, the direction of \mathbf{J} should be defined by angles θ_1 and φ_1 in the “gas reference frame” and by θ_2 and φ_2 in the “grain reference frame” (see Fig. 2). Angle φ_1 describes the precession of \mathbf{J} about magnetic field and angle φ_2 describes the precession of the spheroid’s axis of rotational symmetry about \mathbf{J} . Henceforth grains will be approximated by spheroids with semiaxes a and b .

As the change of grain angular momentum in the course of an individual collision is small, the alignment of \mathbf{J} can be described by the Fokker-Planck equation (see Reichl 1980, Roberge, DeGraff & Flaherty 1993). Then following Dolginov & Mytrophanov (1976), we can write

$$\frac{\partial f(\mathbf{x}, n)}{\partial n} = \sum_{i=0}^2 a_i(\mathbf{x}) \frac{\partial f(\mathbf{x}, n)}{\partial x_i} + \sum_{k,i=0}^2 b_{ik}(\mathbf{x}) \frac{\partial^2 f(\mathbf{x}, n)}{\partial x_i \partial x_k} \quad , \quad (7)$$

where \mathbf{x} is a vector in the phase space with coordinates $J, \cos \theta_1, \cos \theta_2, \varphi_1$ and φ_2 , and the coefficients a_i and b_{ik} obtained on the assumption of supersonic grain drift can be found in Appendix A. The solution of Eq. (7) in the limit of hypersonic drift is (Dolginov & Mytrophanov 1976)

$$f(J, \cos \theta_1, \cos \theta_2, n) = \frac{\text{const}_3}{n^{3/2}} \exp \left(- \frac{J^2(1 + g \cos^2 \theta_2 + s \cos^2 \theta_1)}{2nb^2p^2(1 + g + s)} \right) \quad , \quad (8)$$

where

$$s = - \frac{1}{2} \frac{\langle p^2 \rangle - 3\langle p_z^2 \rangle}{\langle p^2 \rangle - \langle p_z^2 \rangle} \quad (9)$$

is the external flux anisotropy and

$$g = \frac{a^2 - b^2}{2b^2} \quad (10)$$

is the grain non-sphericity. Note, that $\langle p^2 \rangle$ and $\langle p_z^2 \rangle$ are the averaged squared momentum and its Z_1 component (see Fig. 2) transferred to a grain in an individual collision. Both g and s can vary from -0.5 to ∞ . It is easy to see that $g = -0.5$ corresponds to flakes and $g \rightarrow \infty$ to needles; $s = -0.5$ corresponds to a flux perpendicular to magnetic field, while $s \rightarrow \infty$ to a flux parallel to the field. The fluxes are measured in the grain reference frame, and therefore a gaseous flux with the velocity u is equivalent to grain drift with the velocity $-u$ in respect to the ambient gas.

Spherical grains ($g = 0$) correspond to $a = b$, while isotropic fluxes ($s = 0$) to $\langle p^2 \rangle = 3 \langle p_z^2 \rangle$. We expect changes in grain alignment when $s = 0$ and/or $g = 0$. To have a picture which is easy to visualize, we refer to fluxes (drifts) corresponding to $s < 0$ as “fluxes (drifts) at large angles to magnetic field”, and to those corresponding to $s > 0$ as “fluxes (drifts) at small angles to magnetic field”. Note, that “small” angles lie within the interval $[0, \arccos(1/\sqrt{3})]$, while “large” angles in $[\arccos(1/\sqrt{3}), \pi/2]$, if we limit our discussion to the first quadrant. Obviously, oblate and prolate grains correspond to $g < 0$ and $g > 0$, respectively.

Calculations in Dolginov & Mytrophanov (1976) show that the solution given by Eq. (8) is accurate up to $0.25|gs|$ order terms for $|s| < 1$ and $|g| < 1$. The accuracy becomes of the order of s^{-2} when $s \rightarrow \infty$ and $|g| < 0$, whereas it is g^{-2} when $g \rightarrow \infty$ and $s < 0$. If both g and s are large, the accuracy is of the order of $\max[g^{-1}, s^{-1}]$.

Angle $\hat{\theta}$ can be found from simple geometric considerations (see Fig. 2)

$$\cos \hat{\theta} = \cos \theta_1 \cos \theta_2 + \sin \theta_1 \sin \theta_2 \cos(\varphi_1 - \varphi_2) \quad . \quad (11)$$

Averaging out the dependencies on φ_1 and φ_2 provides (see Davis & Greenstein 1951 eq. 108):

$$\langle \cos^2 \hat{\theta} \rangle_\varphi = 0.5(1 - \cos^2 \theta_1 - \cos^2 \theta_2 + 3 \cos^2 \theta_1 \cos^2 \theta_2) \quad . \quad (12)$$

To calculate the Rayleigh reduction factor given by Eq. (2), it is necessary to find $\langle \cos^2 \hat{\theta} \rangle$. After averaging Eq. (8) over J the required distribution function can be found to be

$$W_G(\theta_1, \theta_2) = C(g, s)(1 + g \cos^2 \theta_2 + s \cos^2 \theta_1)^{-\frac{3}{2}} \quad , \quad (13)$$

where $C(g, s)$ is the normalization constant for any fixed s and g . Then

$$\langle \cos^2 \hat{\theta} \rangle = \frac{\iint \cos^2 \hat{\theta} W_G \sin \theta_1 \sin \theta_2 d\theta_1 d\theta_2}{\iint W_G \sin \theta_1 \sin \theta_2 d\theta_1 d\theta_2} \quad . \quad (14)$$

The necessary calculations are performed in Appendix B, and here we present the final expression

$$\langle \cos^2 \hat{\theta} \rangle = \frac{1}{2gs} \left(1 + g + s + gs - C(g, s) \sqrt{1 + g + s} \right) , \quad (15)$$

where

$$C(g, s) = \begin{cases} \sqrt{gs} \left(\arctan \sqrt{\frac{gs}{1+g+s}} \right)^{-1} , & gs > 0 \quad , \\ \sqrt{|gs|} \left(\operatorname{arctanh} \sqrt{\frac{|gs|}{1+g+s}} \right)^{-1} , & gs < 0 \quad , \end{cases} \quad (16)$$

which is valid for all possible values of s and g . This expression can be compared with the analytics found for the case of strong relaxation (see Appendix C).

The corresponding Rayleigh reduction factor is

$$R = \frac{1}{4} + \frac{3\sqrt{1+g+s}}{4gs} \left(\sqrt{1+g+s} - C(g, s) \right) . \quad (17)$$

This measure enters the formulae for intensity of polarized radiation due to dichroic absorption. Equation (17) encompasses a variety of circumstances, which are explored below.

3.2. Comparison with Paper I

Here we discuss the alignment for various values of s and g . When internal dissipation aligns \mathbf{J} and the axis of major inertia perfectly, Eqs. (12), (2) and (1) give the following relation between the Rayleigh reduction factor and the measure of alignment of angular momentum, σ_J , used in Paper I

$$R = \begin{cases} \sigma_J, & \text{for oblate grains} \quad , \\ -0.5\sigma_J, & \text{for prolate grains} \quad . \end{cases} \quad (18)$$

It is easy to see that prolate and oblate grains produce polarization of the same sign despite the fact, that the Rayleigh reduction factor has opposite signs in these two cases. This becomes clear if one recalls that oblate grains align their short axes in respect to the magnetic field, while prolate grains align their long axes.

First, consider oblate grains ($g < 0$) subjected to drift at large angles to magnetic field ($s < 0$). The corresponding measure of alignment is shown in Fig. 3. A comparison with fig. 3 in Paper I reveals the decrease of alignment associated with suppression of internal

dissipation. For instance, for the drift perpendicular to magnetic field lines, this measure for flake-like grains is 0.25 if the Barnett alignment is absent, while it reaches unity (complete alignment) if the internal dissipation is efficient (see Fig. 4).

The alignment measure for oblate grains drifting at small angles to magnetic field ($s > 0$) is shown in Fig. 6. The comparison with fig. 4 in Paper I testifies an order of magnitude decrease of the measure. A cross-section of the plot for $g = -0.5$ (see Fig. 5.) shows that flakes are only marginally aligned. This is in contrast with the case of intense internal dissipation, when flakes are well aligned and the measure of alignment approaches -0.5 , if the flux and magnetic field directions coincide (Lazarian 1994a). Due to the symmetry of the distribution function given by Eq. (8) under a simultaneous interchange $\cos \theta_1 \leftrightarrow \cos \theta_2$ and $s \leftrightarrow g$, we can claim that needles are marginally aligned if grain drift is perpendicular to the field, i.e. $\mathbf{u} \perp \mathbf{B}$. Indeed, the corresponding measure of alignment for prolate grains is negligible (see Fig. 7). In brief, if the internal dissipation is negligible, prolate and oblate grains are marginally aligned for drifts at angles close to $\pi/2$ and 0 , respectively.

When both s and g are positive, the corresponding measure of alignment is shown in Fig. 8. One can see that this measure tends to $+0.25$ when s or/and g tend to infinity. In terms of σ_J (see Eq. (18)) this is equivalent to $\sigma_J = -0.5$ obtained in Paper I. This correspondence has a simple explanation. Indeed, for a needle the angular momentum should be directed along the axis of major inertia even in the absence of internal dissipation.

The requirement of large s and g places stringent constraints on the efficiency of alignment for typical ISM conditions. Indeed, let grain drift velocity components perpendicular and parallel to magnetic field be u_\perp and u_\parallel , respectively, then if u_\perp is much greater than the rms velocity of gas atoms v_{rms}

$$s = \frac{2 - w^2}{2 w^2} \quad , \quad (19)$$

where $w \approx u_\perp/u_\parallel$. If $u_\perp \ll v_{rms}$, then $w \approx v_{rms}/v_\parallel$ should be used in Eq. (19). In any case, w is unlikely to be less than 0.1, and therefore s is not likely to be greater than 100. We neither believe that the axis ratio of a typical prolate grain exceeds 10, therefore g is likely to be less than 50. The measure of alignment for $w \in [0.2, 0.7]$ and the axis ratio $y \equiv a/b \in [1, 10]$ is shown in Fig. 9. The cross-sections of the plot for $y = 5$ and $y = 10$ are shown in Fig. 10.

To summarize, in the absence of internal dissipation, the measure of alignment drops. Oblate grains are most aligned for $\mathbf{u} \perp \mathbf{B}$, and prolate grains are most aligned for $\mathbf{u} \parallel \mathbf{B}$.

4. Generalized problem

Up to now two extreme cases were discussed: strong internal dissipation, when the angular momentum is coupled to the axis of major inertia, and weak internal dissipation, when the residual alignment of angular momentum is due to the differences between the maximal and minimal rotational inertia. In both cases analytical solutions were found. These solutions provide the upper and lower bounds for the measure of alignment. For instance, Fig. 11 shows these two bounds for $\mathbf{u} \perp \mathbf{B}$ when the alignment is caused by ambipolar diffusion. A conspicuous feature of this particular figure is that the two plots are different for ideal spheres, i.e. when no axis alignment is expected. Equation (4) testifies that for $h \rightarrow 1$, all positions of \mathbf{J} become equally probable. This fact was ignored in our simplified approach adopted in Paper I. Fig. 11 also testifies, that the internal dissipation strongly influences grain alignment, as the spread in Rayleigh reduction factors for the two extreme cases is wide.

To account for the incomplete alignment of \mathbf{J} in the grain reference frame, one has to incorporate internal dissipation in the Fokker-Planck equation. An analytical study in this case seems formidable, and a numerical approach, e.g. similar to the one used by Roberge, DeGraff & Floherty (1993) may be advantageous. For such a study both the analytical solutions obtained above and those derive in Paper I should serve as benchmarks.

A less rigorous, but less laborious way to account for the incomplete alignment is to follow Jones & Spitzer (1967). Let the distribution function of \mathbf{J} in the presence of internal dissipation, W_{GD} , be the product of the distribution functions W_{G} and W_{D} given by Eqs (13) and (4), respectively. Then after expressing h in terms of g and J^2 in terms of T_{eff} using Eqs (5) and (6), respectively, we get

$$W_{\text{GD}} \approx \text{const} \times \sin \theta_2 (1 + g \cos^2 \theta_2 + s \cos^2 \theta_1)^{-\frac{3}{2}} \exp \left(\frac{T_{\text{eff}}}{T_s} \frac{g(2g+3)}{g+1} \frac{\sin^2 \theta_2}{2} \right) . \quad (20)$$

Using W_{GD} in Eq. (14) we calculated $\langle \cos^2 \hat{\theta} \rangle$ and the Rayleigh reduction factor for T_{eff}/T_s equal to 100, 10 and 1.1. For example, Fig. 12 shows the Rayleigh reduction factor as a function of grain oblateness. The comparison between Figs 12 and 11 shows that while for efficient internal relaxation corresponding to $T_{\text{eff}}/T_s > 100$ the approximation of perfect coupling is appropriate, in the case of $T_{\text{rot}} \approx T_s$, this is no longer true, and the analytics disregarding internal relaxation provide a better fit. Similar conclusions are valid for other values of s and g with the exception of $g \rightarrow 0$. In this case, as discussed earlier, there is no coupling between the angular momentum and the axis of greatest inertia.

The alignment of prolate grains by ambipolar diffusion is marginal and the comparison between Figs 13 and 7 shows that the internal dissipation does not change it much. In

contrast, Figs 14 and 5 show that the internal dissipation drastically changes the alignment of oblate grains due to the radiation pressure. If this alignment is marginal when the internal relaxation is suppressed (see Fig. 5), it becomes substantial as soon as the internal relaxation is present. This difference in the susceptibility to internal dissipation is easy to understand if one recalls that without internal dissipation \mathbf{J} is only marginally aligned with the axis of major inertia for oblate grains and the alignment is substantial in the case of prolate grains. Therefore Fig. 14 shows a marginal difference in grain alignment for different values of internal dissipation as grains become sufficiently prolate.

To summarize, our results show that Gold alignment is modified by internal relaxation, and to predict the alignment accurately it is essential to estimate the ratio of the effective rotational grain temperature to grain material temperature. Small temperature ratios usually occur when the grain drift and the thermal velocities are comparable.⁷ Then it is essential to account for the fact, that, in the grain reference frame, atoms move at the drift velocity, which is modified by thermal motion. In other words, grain - gas collisions formally correspond to a range of values of s . To account for this effect, we suggest to integrate over the corresponding range of s (see Lazarian 1995a). Since there is no direct numerical calculations of the measure of alignment for the case of incomplete internal relaxation, in what follows we compare our results only with numerics for perfect coupling between \mathbf{J} and the axis of major inertia.

5. Comparison with RHM

A comprehensive numerical study of the Gold alignment for perfect Barnett relaxation was done in RHM. The authors presented a detailed study of grain alignment for a range of drift velocities starting from subsonic ones. Paramagnetic relaxation was also included in their model. Here we briefly discuss how to improve our model to include both subsonic drift and paramagnetic relaxation.

5.1. Subsonic drift

The model adopted here assumes that the grain drift is essentially hypersonic. In other words, we have ignored the rms velocity of gaseous atoms as compared with the drift

⁷We disregard a rather artificial case of hot grains drifting in cold gas.

velocity and assumed that atoms hit the grain from one direction defined by

$$\phi = \arcsin \sqrt{\frac{u_x^2 + u_y^2}{u_x^2 + u_y^2 + u_z^2}} \quad , \quad (21)$$

where u_i , $i= x, y, z$, are the components of atom drift velocity in the grain reference frame. Obviously, the anisotropy parameter s can be expressed as a function of ϕ

$$s = \frac{1 - 3 \cos^2 \phi}{1 - \cos^2 \phi} \quad (22)$$

and hence the Rayleigh reduction too.

When the drift is subsonic, in the grain reference frame atoms are viewed as approaching from various directions, any particular atom at angle

$$\phi = \arcsin \sqrt{\frac{(u_x + v_x)^2 + (u_y + v_y)^2}{(u_x + v_x)^2 + (u_y + v_y)^2 + (u_z + v_z)^2}} \quad , \quad (23)$$

where v_i , $i= x, y, z$, are the components of rms velocity of the atom. According to Eq. (23), angle ϕ varies from atom to atom due to variations in v_i . To obtain the statistics of R we subdivide atoms into subgroups of atoms having the same v_i .⁸ For each of the subgroups, ϕ is constant, hence the measure of alignment can be obtained by averaging $R(u_i, v_i)$ over a Maxwell-Boltzmann distribution of v_i .

Elsewhere we hope to test the applicability of such an approach for a considerable range of drift velocities by comparing our predictions with direct numerical simulations. At the moment, we want to show that our estimates are in a reasonable agreement with the data presented in RHM.

RHM assume that the angular momentum is perfectly coupled with the axis of major inertia, which corresponds to $T_s/T_{\text{eff}} = 0$ in our model. The effect of the spread of atom velocities in the grain reference frame should not depend upon the position of the angular momentum in respect to the axis of the major inertia. Indeed, the velocities of particles on the grain surface are much smaller than the velocities of striking atoms and therefore if we obtain the correspondence between our and RHM predictions we may hope that our treatment is applicable when the internal alignment is incomplete.

Figure 8 in RHM shows the Rayleigh reduction factor for oblate grains drifting with different velocities in respect to gas. The calculations are made up to Mach number 4, but

⁸As the time of alignment is much shorter than the damping time (see Paper I), each of the subgroups may by itself cause alignment.

the saturation of the alignment is obvious from this plot. Therefore we will consider that these values correspond to hypersonic velocities and define $R(\phi_0)$, where ϕ_0 in the case of ambipolar diffusion studied in RHM is $\pi/2$. For our simplified estimates we observe that for large Mach numbers M , Eq. (23) provides

$$\phi \approx \arcsin\left(1 - 0.5 M^{-2}\right) \approx \frac{\pi}{2} - \frac{1}{2}M^{-2} - \frac{\sqrt{2}}{24}M^{-3} \quad , \quad (24)$$

where the first term corresponds to ϕ_0 and the rest can be interpreted as $\delta\phi$. Therefore

$$\langle R \rangle_\phi \approx \frac{1}{2\delta\phi} \int_{\phi_0-\delta\phi}^{\phi_0+\delta\phi} R(\phi) d\phi \approx R(\phi_0) + 2 \frac{dR}{ds} \frac{ds}{d\phi} \delta\phi \quad , \quad (25)$$

where

$$R(\phi_0) = -3.5 - 3g + 3 \sqrt{1+2g} (1+g) \arcsin \frac{1}{2\sqrt{1+g}} \quad , \quad (26)$$

$$\begin{aligned} \left. \frac{dR}{ds} \right|_{s=-0.5} &= \frac{3+3g}{\sqrt{1+2g}\sqrt{3+4g}} \left[-1 - 2g - 2\sqrt{1+2g}\sqrt{3+4g} \right. \\ &\quad \left. + \sqrt{3+4g} (4+6g) \arcsin \left(\frac{1}{2\sqrt{1+g}} \right) \right] \quad , \quad (27) \end{aligned}$$

and

$$\frac{ds}{dx} = \frac{6 \cos x \sin x}{1 - \cos^2 x} - \frac{(2 - 6 \cos^2 x) \cos x \sin x}{(1 - \cos^2 x)^2} \quad , \quad (28)$$

with $ds/dx \approx 0.032$ when $x = \phi = \pi/2$.

For instance, RHM find that at large Mach numbers the Rayleigh reduction factor for grains with the axis ratio 0.5 is ≈ 0.25 . This axis ratio corresponds to $g = 1.7$, when plugged into Eq. (25) it gives $\langle R \rangle_\phi \approx 0.21$ for $M = 2$. This is comparable with the value ≈ 0.19 that follows from fig. 8 in RHM. Similarly for the axis ratio 0.25 corresponding to $g = 7.5$, $\langle R \rangle_\phi \approx 0.27$, for $M = 2$, which is of the same order, as the result in RHM (≈ 0.26).⁹ As the values of the Rayleigh reduction factor obtained in RHM for high Mach numbers essentially correspond to the values obtained in the analytical treatment in Paper I (see fig. 12 in RHM) it is possible to see, that a purely analytical treatment is appropriate at least for some values of subsonic drift velocities. The entire range of velocities will be treated elsewhere.

⁹Again we take the values of the Rayleigh reduction factor obtained for $M = 4$ in RHM and substitute in our formulae. For the axis ratio 0.25 this value ≈ 0.39 .

Our estimates above were obtained using the analytical solutions obtained in Paper I for perfect coupling of \mathbf{J} with the axis of major inertia. Evidently our approach is also applicable to describe alignment at low Mach numbers using the analytics and “semi-analytics” obtained in Sections 3 and 4 respectively. We are looking forward to the progress in numerical techniques to be able to compare our predictions with the results of direct numerical simulations.

5.2. Mechanical and paramagnetic alignment

So far we have talked only about mechanical alignment and completely disregarded the paramagnetic one. This is justifiable only if the Davis-Greenstein alignment is negligible. In general, the Davis-Greenstein alignment must be accounted for. To do this we propose a simple formula.

If we denote the Rayleigh reduction factor of the Gold alignment by R_G , the measure of the internal alignment by Q_X , and that of Davis-Greenstein process by R_{DG} , it is possible to estimate the measure of the overall alignment as

$$R^\Sigma \approx Q_X \frac{Q_X \sigma_G + R_G R_{DG} + Q_X R_{DG}}{Q_X^2 + 2R_G R_{DG}} \quad . \quad (29)$$

To obtain the expression above we used the expression for J alignment given by eq. 45 in Lazarian (1995a) and the approximation

$$R_i \approx Q_{J(i)} \times Q_X \quad , \quad (30)$$

where R_i is the Rayleigh reduction factor obtained for the i mechanism acting alone, while $Q_{J(i)}$ is the measure of J alignment relatively to magnetic field. The latter approximation follows from spherical trigonometry (see Eq. (12)). Indeed, if two processes are independent, then

$$\langle \cos^2 \theta_1 \cos^2 \theta_2 \rangle \approx \langle \cos^2 \theta_1 \rangle \langle \cos^2 \theta_2 \rangle \quad . \quad (31)$$

The approximation above was proved to be sufficiently accurate for the Davis-Greenstein process in Lazarian (1995a), but may be much less accurate for the Gold alignment. In any case, we treat Eq. (29) only as a conjecture to be tested in future.

A study of the simultaneous action of the paramagnetic and mechanical alignment has been done recently in RHM for $T_d/T_g = 0$. In this case, $\sigma_B \equiv 1$ and Eq. (29) reduces to the one derived in Lazarian (1995a).

First of all, to provide the comparison we must define the measure of alignment for the Davis-Greenstein process when grains are subjected to a supersonic flow. Naturally, as

grains drift faster the rate at which atoms arrive to their surface increases, and therefore the gaseous damping time decreases. For our rough estimate of the Davis-Greenstein alignment subjected to the supersonic flow, we simply substitute overall velocity instead of the thermal one into the expressions for the diffusion coefficients for gaseous bombardment (see Roberge, DeGraff & Flaherty 1993). This changes both T_{eff} and the ratio of the gaseous and magnetic damping times δ_1 (see eq. 25 in Lazarian 1995). The first change is not relevant here because to compare our estimates with the calculations in RHM, we assume $T_s/T_{\text{eff}} = 0$. On the contrary, the second change rescales δ_1 calculated for the non-drifting grain (this value is shown in figs 4 and 9 in RHM). Let the rescaled value be δ/M . To obtain σ_G , we use the zero approximation in Lazarian (1995c).

For spherical grains when $\delta_1 = 10$, RHM obtain $\sigma \approx 0.40$ (see fig. 4 in RHM). Our approximation gives $\sigma \approx 0.38$. It is easy to see from fig. 9 in RHM that for $\delta_1 = 1$, axis ratio 0.5 gives $\sigma \approx 0.32$, whereas axis ratio 0.25 gives $\sigma \approx 0.48$. Our approach provides $\sigma \approx 0.29$ and 0.46, respectively. This approximate correspondence let us hope that our simplified analytical treatment reproduces essential features of the alignment.

6. Discussion

In short, we have shown that the alignment of \mathbf{J} in the grain reference frame, that arises from the difference between the grain material and rotational temperatures, is essential for the Gold alignment. When velocities of grain drift are hypersonic, we can assume perfect coupling of \mathbf{J} and the axis of major inertia. However, this assumption fails for mildly supersonic drifts when the gas and grain temperatures are comparable. Such conditions are expected, e.g. in molecular clouds undergoing ambipolar diffusion. Then incomplete alignment between \mathbf{J} and the axis of major inertia should be accounted for.

Our results also show that the effect of incomplete relaxation is more vivid for oblate grains than for prolate ones. This is a consequence of the fact, that for sufficiently prolate grains the alignment of \mathbf{J} in respect to grain axis of major inertia is manifest even without internal relaxation.

The analytical results obtained above and those derived in Paper I provide the lower and upper bounds for Gold alignment. In a general case of incomplete internal alignment, we suggested a semi-analytical approach.

To provide a quantitative description of Gold alignment for drift velocities comparable with the thermal velocities of gaseous atoms, we suggested an expansion of Rayleigh reduction factor in a series over the drift Mach number and obtained a fair correspondence

with the results of direct numerical computations.

Comments by Bruce Draine initiated this work, but its completion would not be possible if not for the encouragement by Ethan Vishniac. I am indebted to Wayne Roberge for his constructive criticism of the initial draft. Present work was partially done during my stay in the stimulating environment of Harvard-Smithsonian Observatory and I gratefully acknowledge a Short-Term Visitor Fellowship from the Smithsonian Institution and hospitality of Phil Myers. The research is supported by NASA grant NAG5 2773 at the University of Texas at Austin.

A. Coefficients of the Fokker-Planck equation

The coefficients a_i and b_{ik} of the Fokker-Planck equation are determined by the change of the grain angular momentum due to grain - atom collision

$$a_0 = \left\langle \frac{1}{2} \Delta x_2 \frac{\partial \Delta x_1}{\partial x_2} + \frac{1}{2} \Delta \varphi_1 \frac{\partial \Delta x_1}{\partial \varphi_1} - \Delta x_1 \right\rangle , \quad (\text{A1})$$

$$a_m = \left\langle \frac{1}{2} \Delta x_1 \frac{\partial \Delta x_m}{\partial x_1} + \frac{1}{2} \Delta x_m \frac{\partial \Delta x_m}{\partial x_m} + \frac{1}{2} \Delta \varphi_m \frac{\partial \Delta x_m}{\partial \varphi_m} - \Delta x_m \right\rangle , \quad (\text{A2})$$

$$b_{ik} = \langle \Delta x_i \Delta x_k \rangle , \quad (\text{A3})$$

where $m = 1, 2$, $k, i = 0, 1, 2$, and the angular brackets denote averaging over atom impacts over the grain surface. The quantities Δx_i and $\Delta \varphi_i$ and the corresponding a_i and b_{ik} were calculated in Dolginov & Mytrophanov (1976) using the following equations:

$$\begin{aligned} \Delta x_j &= \Delta(\mathbf{e}_j \cdot \mathbf{J}) - (\mathbf{e}_j \cdot \mathbf{J}) \Delta J , \\ \Delta x_0 &= \mathbf{j} \cdot \Delta \mathbf{J} , \\ \Delta \varphi_j &= ((\mathbf{e}_j \times \mathbf{j}) \cdot \Delta \mathbf{J} (J(1 - x_j^2))^{-1}) , \end{aligned}$$

where $j = 1, 2$, $\mathbf{e}_1 = \mathbf{H}/|\mathbf{H}|$ is a unit vector along the magnetic field, $\mathbf{e}_2 = \mathbf{a}/|\mathbf{a}|$ is a unit vector along Z_1 -axis of the grain, $\mathbf{j} = \mathbf{J}/|\mathbf{J}|$ is a unit vector along \mathbf{J} , and $\Delta \mathbf{J} = \mathbf{r} \times \mathbf{p}$ with \mathbf{r} and \mathbf{p} used for the vector to the point of atomic impact and atom momentum, respectively.

To find coefficients a_k ($k = 0, 1, 2$) and b_{ik} ($i, k = 0, 1, 2$) (see Dolginov & Mitrophanov 1976, eq. 5) one has to substitute Δx_j , Δx_0 , $\Delta \varphi_j$ into Eqs (A1), (A2), and (A3) and perform the necessary averaging. Apart from averaging over the surface area exposed to the flux, one has to average over the angles of precession of \mathbf{J} about \mathbf{e}_2 and \mathbf{m} .

B. Computation of integrals

Equation (14) involves integration of Eq. (13) with the distribution function $W_G(\theta_1, \theta_2)$. As a result, we get

$$\langle \cos^2 \theta \rangle = 0.5 \left(1 - \langle \cos^2 \theta_1 \rangle - \langle \cos^2 \theta_2 \rangle + 3\langle \cos^2 \theta_1 \cos^2 \theta_2 \rangle \right) , \quad (\text{B1})$$

where the explicit expression for the first term is

$$\langle \cos^2 \theta_1 \rangle = C(g, s) \int_0^{\pi/2} d\theta_1 \int_0^{\pi/2} \frac{\cos^2 \theta_1 \sin \theta_1 \sin \theta_2}{(1 + s \cos^2 \theta_1 + g \cos^2 \theta_2)^{3/2}} d\theta_2 . \quad (\text{B2})$$

After integrating over θ_2 and the change of variables, $\sin \theta_1 = x$, we have

$$\langle \cos^2 \theta_1 \rangle = C(g, s) \int_0^1 \frac{x^2 dx}{(1 + sx^2)\sqrt{1 + sx^2 + g}} , \quad (\text{B3})$$

where

$$C(g, s) \int_0^1 \frac{dx}{(1 + sx^2)\sqrt{1 + sx^2 + g}} \equiv 1 . \quad (\text{B4})$$

Using the identity

$$\frac{1}{s}(1 + sx^2) - \frac{1}{s} = x^2 , \quad (\text{B5})$$

Equation (B3) reduces to

$$\langle \cos^2 \theta_1 \rangle = C(g, s) \frac{1}{s} \int_0^1 \frac{dx}{\sqrt{1 + sx^2 + g}} - \frac{1}{s} , \quad (\text{B6})$$

which can be calculated [Gradshteyn & Ryzhik 1965, 2.271(4)] to give

$$i_1 = \int_0^1 \frac{dx}{\sqrt{(1+g) + sx^2}} = \begin{cases} \frac{1}{\sqrt{s}} \ln \frac{\sqrt{s} + \sqrt{1+g+s}}{\sqrt{1+g}}, & s > 0 \\ \frac{1}{\sqrt{-s}} \arcsin \sqrt{-\frac{s}{1+g}}, & s < 0 \end{cases} . \quad (\text{B7})$$

For uniform representation, one can also use inverse hyperbolic function for $s < 0$, namely

$$i_1 = \frac{1}{\sqrt{s}} \operatorname{arcsinh} \sqrt{\frac{s}{1+g}}, \quad (\text{B8})$$

where

$$\operatorname{arcsinh} z = \ln(z + \sqrt{z^2 + 1}) = \frac{1}{i} \arcsin (iz). \quad (\text{B9})$$

To find $C(g, s) = i_2^{-1}$, we calculate

$$i_2 = \int_0^1 \frac{dx}{(1 + sx^2)\sqrt{1 + sx^2 + g}} . \quad (\text{B10})$$

By substituting $u = x^2 + s$ into Eq. (B10) and evaluating the resulting integral (Gradshteyn & Ryzhik 1965, 2.224(5)), we have

$$i_2 = \begin{cases} \frac{1}{2\sqrt{-gs}} \ln \frac{\sqrt{1+s+g} + \sqrt{-gs}}{\sqrt{1+s+g} - \sqrt{-gs}}, & gs < 0 \quad , \\ \frac{1}{\sqrt{gs}} \arctan \sqrt{\frac{gs}{1+s+g}}, & gs > 0 \quad . \end{cases} \quad (\text{B11})$$

Using the inverse hyperbolic function

$$\operatorname{arctanh} z = \frac{1}{2} \ln \frac{1+z}{1-z} = \operatorname{arctan}(iz) \quad , \quad (\text{B12})$$

the expression for i_2 can be rewritten as

$$i_2 = \frac{1}{\sqrt{-gs}} \operatorname{arctanh} \sqrt{\frac{-gs}{1+s+g}}, \quad sg < 0 \quad . \quad (\text{B13})$$

Finally, we obtain,
for $s < 0$ and $g < 0$,

$$\langle \cos^2 \theta_1 \rangle = \frac{\sqrt{-g} \arcsin \sqrt{\frac{-s}{1+g}}}{s \arctan \sqrt{\frac{gs}{1+s+g}}} - \frac{1}{s} \quad , \quad (\text{B14})$$

for $s < 0$, and $g > 0$,

$$\langle \cos^2 \theta_1 \rangle = \frac{\sqrt{g} \arcsin \sqrt{\frac{-s}{1+g}}}{s \operatorname{arctanh} \sqrt{\frac{-gs}{1+s+g}}} - \frac{1}{s} \quad , \quad (\text{B15})$$

for $s > 0$, and $g < 0$,

$$\langle \cos^2 \theta_1 \rangle = \frac{\sqrt{-g} \operatorname{arcsinh} \sqrt{\frac{s}{1+g}}}{s \operatorname{arctanh} \sqrt{\frac{-gs}{1+s+g}}} - \frac{1}{s} \quad , \quad (\text{B16})$$

for $s > 0$, and $g > 0$,

$$\langle \cos^2 \theta_1 \rangle = \frac{\sqrt{g} \operatorname{arcsinh} \sqrt{\frac{s}{1+g}}}{s \arctan \sqrt{\frac{sg}{1+s+g}}} - \frac{1}{s} \quad , \quad (\text{B17})$$

which covers all cases. Similarly, for the second term in Eq. (B1) we obtain

$$\langle \cos^2 \theta_2 \rangle = \begin{cases} C(g, s) \frac{1}{g\sqrt{-g}} \arcsin \sqrt{\frac{-g}{1+s}}, & g < 0 \quad , \\ C(g, s) \frac{1}{g\sqrt{g}} \operatorname{arcsinh} \sqrt{\frac{g}{1+s}}, & g > 0 \quad . \end{cases} \quad (\text{B18})$$

The last term in Eq. (B1) is

$$\langle 3 \cos^2 \theta_1 \cos^2 \theta_2 \rangle = 3C(g, s) \int_0^{\pi/2} \int_0^{\pi/2} \frac{\cos^2 \theta_1 \cos^2 \theta_2 \sin \theta_1 \sin \theta_2 d\theta_1 d\theta_2}{(1 + s \cos^2 \theta_1 + g \cos^2 \theta_2)^{3/2}} \quad , \quad (\text{B19})$$

which after obvious substitutions takes the form

$$\langle 3 \cos^2 \theta_1 \cos^2 \theta_2 \rangle = 3C(g, s) \int_0^1 x^2 dx \int_0^1 \frac{y^2 dy}{(1 + sx^2 + gy^2)^{3/2}} . \quad (\text{B20})$$

Let $s < 0$ and $g < 0$, then

$$\begin{aligned} s &= -b^2 , \\ g &= -d^2 , \end{aligned} \quad (\text{B21})$$

for some non-zero b and d . Which gives for the inner integral in Eq. (B20)

$$\begin{aligned} G_1 &= \int_0^1 \frac{y^2 dy}{(1 - b^2 x^2 - d^2 y^2)^{3/2}} = \left[\frac{y}{d^2 \sqrt{1 - b^2 x^2 - d^2 y^2}} - \frac{1}{d^3} \arcsin \frac{dy}{\sqrt{1 - b^2 x^2}} \right]_0^1 \\ &= \frac{1}{d^2 \sqrt{1 - b^2 x^2 - d^2 y^2}} - \frac{1}{d^3} \arcsin \frac{d}{\sqrt{1 - b^2 x^2}} . \end{aligned} \quad (\text{B22})$$

Therefore

$$\langle 3 \cos^2 \theta_1 \cos^2 \theta_2 \rangle = \frac{3C(g, s)}{d^2} \left\{ \int_0^1 \frac{x^2 dx}{\sqrt{1 - d^2 - b^2 x^2}} - \frac{1}{d} \int_0^1 x^2 \arcsin \frac{d}{\sqrt{1 - b^2 x^2}} dx \right\} . \quad (\text{B23})$$

The second integral in the square brackets can be integrated by parts

$$\begin{aligned} G_2 &= \frac{1}{d} \int_0^1 x^2 \arcsin \frac{d}{\sqrt{1 - b^2 x^2}} dx \\ &= \frac{1}{3} \left[\frac{1}{d} \arcsin \frac{d}{\sqrt{1 - b^2 x^2}} - \frac{db^2}{d} \int_0^1 \frac{x^4 dx}{(1 - b^2 x^2) \sqrt{1 - d^2 - b^2 x^2}} \right] , \end{aligned} \quad (\text{B24})$$

where

$$\left(\arcsin \frac{d}{\sqrt{1 - b^2 x^2}} \right)' = \frac{db^2 x}{(1 - b^2 x^2) \sqrt{1 - d^2 - b^2 x^2}} \quad (\text{B25})$$

was taken into account. The last integral in Eq. (B24) can be evaluated using the identity

$$-b^2 x^4 = -x^2(b^2 x^2 - 1) - x^2 . \quad (\text{B26})$$

Indeed

$$-\int_0^1 \frac{b^2 x^4 dx}{(1 - b^2 x^2) \sqrt{1 - d^2 - b^2 x^2}} = \int_0^1 \frac{x^2 dx}{\sqrt{1 - d^2 - b^2 x^2}} - \int_0^1 \frac{x^2 dx}{(1 - b^2 x^2) \sqrt{1 - d^2 - b^2 x^2}} . \quad (\text{B27})$$

Thus

$$\begin{aligned} \langle 3 \cos^2 \theta_1 \cos^2 \theta_2 \rangle &= \frac{C(g, s)}{d^2} \left\{ 2 \int_0^1 \frac{x^2 dx}{\sqrt{1 - d^2 - b^2 x^2}} - \frac{1}{d} \arcsin \frac{d}{\sqrt{1 - b^2}} \right. \\ &\quad \left. + \int_0^1 \frac{x^2 dx}{(1 - b^2 x^2) \sqrt{1 - d^2 - b^2 x^2}} \right\} , \end{aligned} \quad (\text{B28})$$

which gives

$$\begin{aligned} \langle 3 \cos^2 \theta_1 \cos^2 \theta_2 \rangle &= C(g, s) \left\{ -\frac{\sqrt{1-d^2-b^2}}{b^2} + \frac{1-d^2}{b^3} \arcsin \frac{b}{\sqrt{1-d^2}} \right. \\ &\quad \left. - \frac{1}{d} \arcsin \frac{d}{\sqrt{1-b^2}} - \frac{1}{b^3} \arcsin \frac{b}{\sqrt{1-d^2}} + \frac{1}{C(g, s)b^2} \right\} . \end{aligned} \quad (\text{B29})$$

Finally,

$$\begin{aligned} \langle 3 \cos^2 \theta_1 \cos^2 \theta_2 \rangle &= C(g, s) \left\{ -\frac{\sqrt{1-d^2-b^2}}{d^2b^2} - \frac{1}{b^3} \arcsin \frac{b}{\sqrt{1-d^2}} \right. \\ &\quad \left. - \frac{1}{d^3} \arcsin \frac{d}{\sqrt{1-b^2}} + \frac{1}{C(g, s)d^2b^2} \right\} , \end{aligned} \quad (\text{B30})$$

which is symmetric in respect to the interchange $g \leftrightarrow s$ if both parameters are negative.

The symmetry breaks if the parameters have opposite signs. Let

$$\begin{aligned} s &= b^2 , \\ g &= -d^2 , \end{aligned} \quad (\text{B31})$$

then one has to calculate

$$\begin{aligned} I_3 &= C(g, s) \left\{ 2 \int_0^1 \frac{x^2 dx}{\sqrt{1-d^2+b^2x^2}} + \int_0^1 \frac{x^2 dx}{(1+b^2x^2)\sqrt{1-d^2+b^2x^2}} \right. \\ &\quad \left. - \frac{1}{d} \arcsin \frac{d}{\sqrt{1+b^2}} \right\} . \end{aligned} \quad (\text{B32})$$

The result is

$$\begin{aligned} I_3 &= \frac{C(g, s)}{d^2} \left\{ \frac{\sqrt{1-d^2+b^2}}{b^2} - \frac{1-d^2}{b^3} \ln \left| \frac{b + \sqrt{1-d^2+b^2}}{\sqrt{1-d^2}} \right| \right. \\ &\quad \left. + \frac{1}{b^3} \ln \frac{b + \sqrt{1-d^2+b^2}}{\sqrt{1-d^2}} - \frac{1}{b^2 C(g, s)} - \frac{1}{d} \arcsin \frac{d}{\sqrt{1+b^2}} \right\} . \end{aligned} \quad (\text{B33})$$

If s is negative while g is positive, the integral is

$$\begin{aligned} I_3 &= \frac{C(g, s)}{b^2} \left\{ -\frac{\sqrt{1+d^2-b^2}}{d^2} - \frac{1-b^2}{d^3} \ln \left| \frac{d + \sqrt{1+d^2-b^2}}{\sqrt{1-d^2}} \right| \right. \\ &\quad \left. + \frac{1}{d^3} \ln \frac{d + \sqrt{1+d^2-b^2}}{\sqrt{1-d^2}} - \frac{1}{d^2 C(g, s)} - \frac{1}{b} \arcsin \frac{b}{\sqrt{1+d^2}} \right\} . \end{aligned} \quad (\text{B34})$$

For s and g both positive, one can obtain the integral by changing the inverse trigonometric functions with inverse hyperbolic functions:

$$\begin{aligned} I_3 &= C(g, s) \left\{ -\frac{\sqrt{1+d^2+b^2}}{b^2d^2} + \frac{1}{b^3} \operatorname{arcsinh} \frac{b}{\sqrt{1+d^2}} \right. \\ &\quad \left. + \frac{1}{d^3} \operatorname{arcsinh} \frac{d}{\sqrt{1+b^2}} + \frac{1}{C(g, s)d^2b^2} \right\} . \end{aligned} \quad (\text{B35})$$

Note that this expression is also symmetric in respect to $s \leftrightarrow g$ interchange. The following formula valid for all values of s and g , sums up our results

$$\langle \cos^2 \hat{\theta} \rangle = \frac{1}{2gs} \left(1 + g + s + gs - C(g, s) \sqrt{1 + g + s} \right) \quad . \quad (\text{B36})$$

Note, that $C(g, s)$ is given by Eq. (16) completely defines the solution for $\langle \cos^2 \hat{\theta} \rangle$.

C. Analytics for perfect coupling

Analytical solutions for the alignment measure corresponding to perfect coupling of \mathbf{J} with the axis of major inertia were obtained in Paper I. Here we write down those solutions in the form convenient for comparing with the solutions obtained in the main body of the present paper.

For oblate grains,

$$\sigma = -\frac{3(1+g)}{2s} \left(1 - \sqrt{-\frac{1+s+g}{s}} \arcsin \sqrt{-\frac{s}{1+g}} \right) - \frac{1}{2}, \quad s < 0 \quad . \quad (\text{C1})$$

and

$$\begin{aligned} \sigma = & -\frac{3(1+g)}{4s^{3/2}} \left[2s^{1/2} + (1+s+g)^{1/2} \right. \\ & \left. \times (\ln(1+g) - 2 \ln(s^{1/2} + (1+s+g)^{1/2})) \right] - \frac{1}{2}, \quad s > 0 \quad . \quad (\text{C2}) \end{aligned}$$

REFERENCES

- Aitken D.K., Smith C.H., Moore T.J.T., Roche P.F. 1995, MNRAS, 273, 359
- Cugnon P. 1985, A&A, 152, 1
- Davis J. 1955, *Vistas in Astronomy*, ed. A. Beer, 1, 336.
- Davis J. & Greenstein J.L. 1951, ApJ, 114, 206
- Dolginov A.Z. & Mytrophanov I.G. 1976, *Ap&SS*, 43, 291
- Dotson J.L. 1995, ApJ, (in press)
- Eaton N., Scarrott S.M. & Draper P.W. 1995, MNRAS, 273, L59
- Gold T. 1951, Nat, 169, 322
- Gold T. 1952, MNRAS, 112, 215
- Goodman A.A., Jones T.J., Lada E.A., Myers P.C. 1995, ApJ, 448, 748
- Gradstein I.S. & Ryzhik I.M. 1965, *Table of Integrals, Series and Products*, Academic Press, New York
- Greenberg J.M. 1968, in *Nebulae and Interstellar Matter*, Kuiper G.P. & Middlehurst B.M. (eds.), Univ. of Chicago Press, vol. 7
- Hildebrand R.H. 1988, QJRAS, 29, 327
- Hildebrand R.H., & Dragovan M. 1995, ApJ, 450, 663
- Jones R.V. & Spitzer L., Jr 1967, ApJ, 147, 943
- Kwok S. 1975, ApJ, 198, 583
- Lazarian A. 1994, MNRAS, 268, 713
- Lazarian A. 1995a, ApJ, 451, 660
- Lazarian A. 1995b, MNRAS, 277, 1235
- Lazarian, A. 1995c, ApJ, 453, 229
- Lazarian, A. & Efrimsky, M. 1996a ApJ, 466, 274
- Lazarian, A., Efrimsky, M. & Ozik J. 1996b ApJ(in press)

- Lazarian, A. & Roberge, W.G. 1997 ApJ(accepted)
- Martin P.G. 1971, MNRAS, 153, 279
- Mathis J.S. 1986, ApJ, 308, 281
- Purcell E.M. 1969, On the Alignment of Interstellar Dust, *Physica*, 41, 100
- Purcell E.M. 1979, ApJ, 231, 404
- Purcell E.M. & Spitzer L., Jr 1971, ApJ, 167, 31
- Reichl L.E. 1980, Modern Course in Statistical Physics, Edward Arnold (Publishers) Ltd.,
p 168
- Roberge, W.G. 1996 in Polarimetry of the Interstellar Medium, eds Roberge W.G. and
Whittet, D.C.B. p. 401
- Roberge W.G., DeGraff T.A. & Flaherty J.E. 1993, ApJ, 418, 287
- Roberge W.G. & Hanany S. 1990, BAAS, vol.22, p.862
- Roberge W.G., Hanany S. & Messinger D.W., 1995 ApJ, 453, 238
- Spitzer L., Jr 1978, Physical Processes in the Interstellar Medium, Wiley-Interscience Publ.,
New York
- Spitzer L., Jr & McGlynn T.A. 1979, ApJ, 231, 417
- Whittet D.C.B. 1992, Dust in the Galactic Environment, Bristol Inst. Physics

Figure Captions

Fig. 1. Distribution function of J in the grain reference frame for $T_{\text{eff}}/T_s = 100$

Fig. 2. Z_1 axis of the external or gas reference frame, $X_1Y_1Z_1$, is directed along magnetic field. The internal or grain frame, $X_2Y_2Z_2$, is defined so that Z_2 coincides with the symmetry axis of the spheroid. $\theta_1, \varphi_1, \theta_2$, and φ_2 are the polar angles in the above frames.

Fig. 3. Rayleigh reduction factor, R , for oblate grains ($g < 0$) subjected to a flux with $s < 0$. A sharp peak corresponds to $g = s = -0.5$.

Fig. 4. Rayleigh reduction factor, R , for oblate grains ($g < 0$) under MHD waves ($s = -0.5$). The alignment is most efficient for flakes ($g = -0.5$). Due to the intrinsic symmetry inherent to the problem the same plot represents the Rayleigh reduction factor for flakes ($g = -0.5$) when s varies from -0.5 to 0 along the x -axis.

Fig. 5. Rayleigh reduction factor, R , for flakes ($g = -0.5$) under streaming motions corresponding to $s > 0$. Evidently such an alignment is inefficient.

Fig. 6. Rayleigh reduction factor, R , for oblate grains ($g < 0$) when $s > 0$. The alignment measure for prolate grains when $s < 0$ can be obtained simply by inchanging s and g .

Fig. 7. Rayleigh reduction factor, R , for prolate grains ($g > 0$) if $\mathbf{u} \perp \mathbf{B}$ ($s = -0.5$). The alignment is marginal.

Fig. 8. Rayleigh reduction factor, R , for prolate grains ($g < 0$) and $s > 0$. This situation corresponds to the alignment through streaming along magnetic field lines.

Fig. 9. The measure of alignment, R , for prolate grains streaming along magnetic field lines as a function of grain axis ratio y and the velocity ratio w . High degree of alignment corresponds to both large y and small w .

Fig. 10. Rayleigh reduction factor R of prolate grains streaming along magnetic field lines for $y = 10$ (upper plot) and for $y = 5$ (lower plot) for a wide range of the velocities

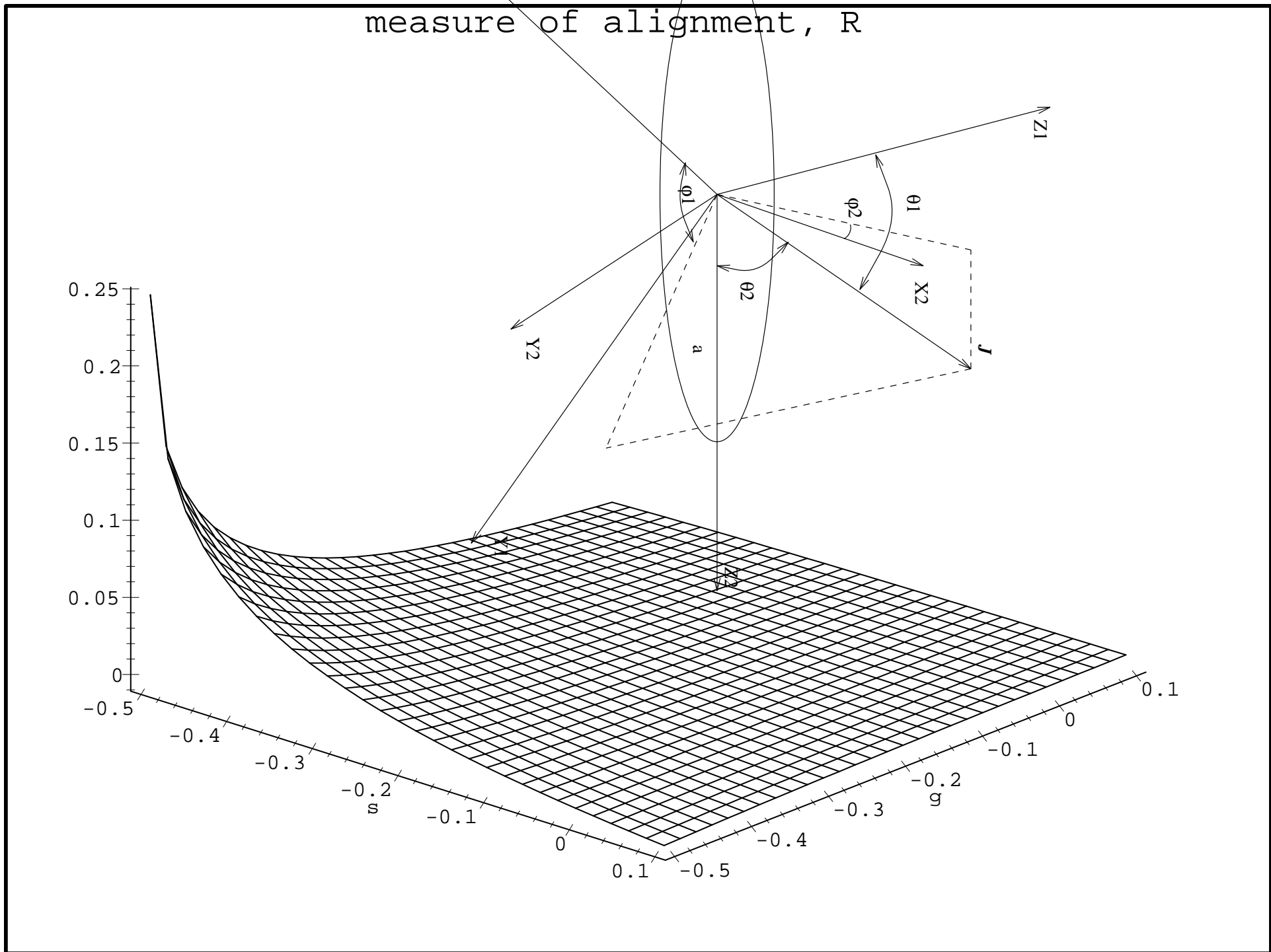
ratio w . It is evident, that for mildly supersonic drift the alignment is marginal.

Fig. 11. Rayleigh reduction factor R of oblate grains subjected to the drift with $\mathbf{u} \perp \mathbf{B}$ for \mathbf{J} coupled with the axis of major inertia as a result of internal dissipation (upper plot) and for negligible internal dissipation (lower plot).

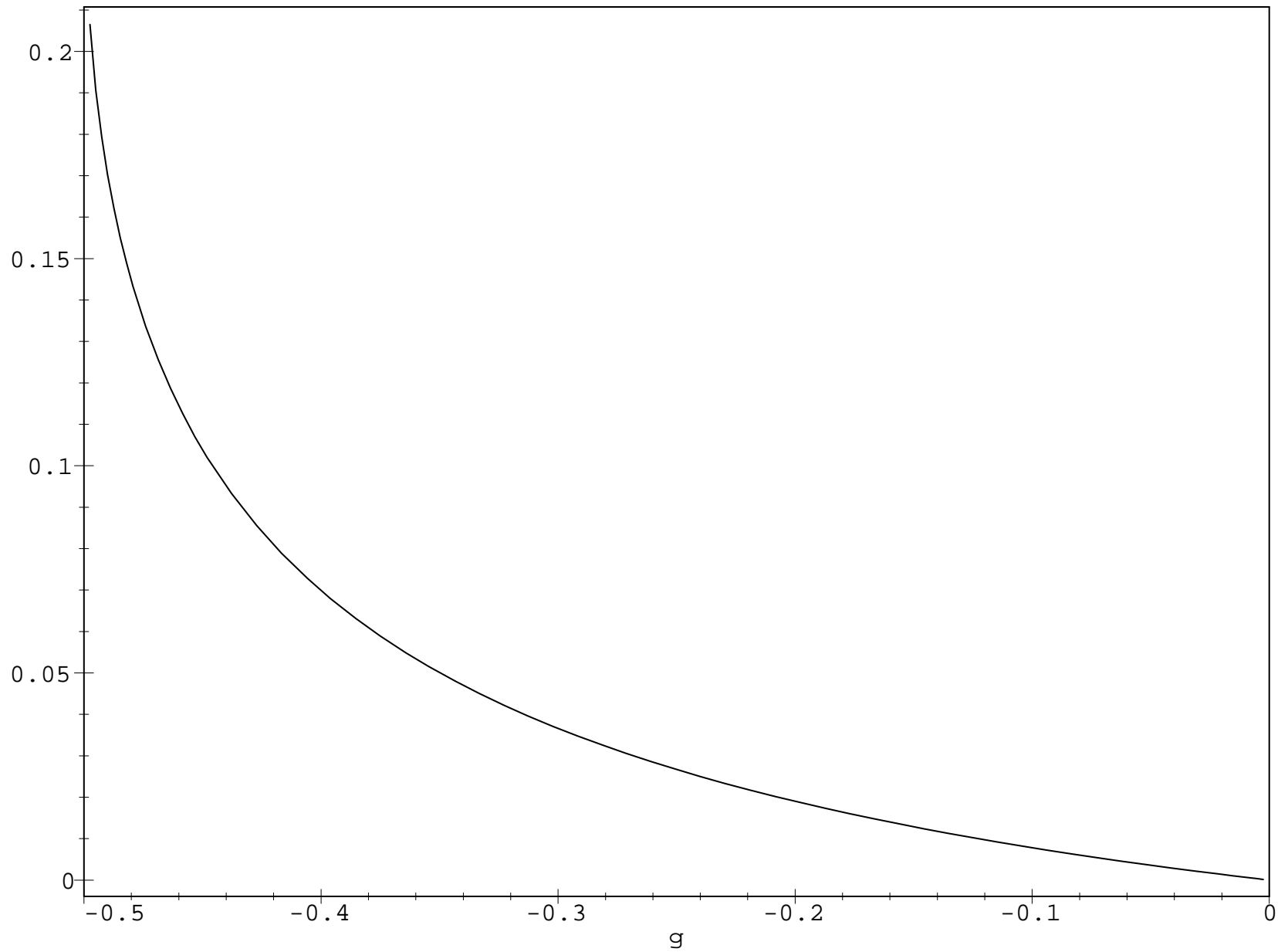
Fig. 12. Rayleigh reduction factor of oblate grains subjected to drift with $\mathbf{u} \perp \mathbf{B}$. The solid line corresponds to the temperature ratio 100, the dotted line corresponds to 10 and the dashed line corresponds to 1.1.

Fig. 13. Rayleigh reduction factor for $\mathbf{u} \perp \mathbf{B}$ as a function of grain eccentricity for prolate grains. The solid line corresponds to the temperature ratio 100, the dotted line corresponds to 10 and the dashed line corresponds to 1.1.

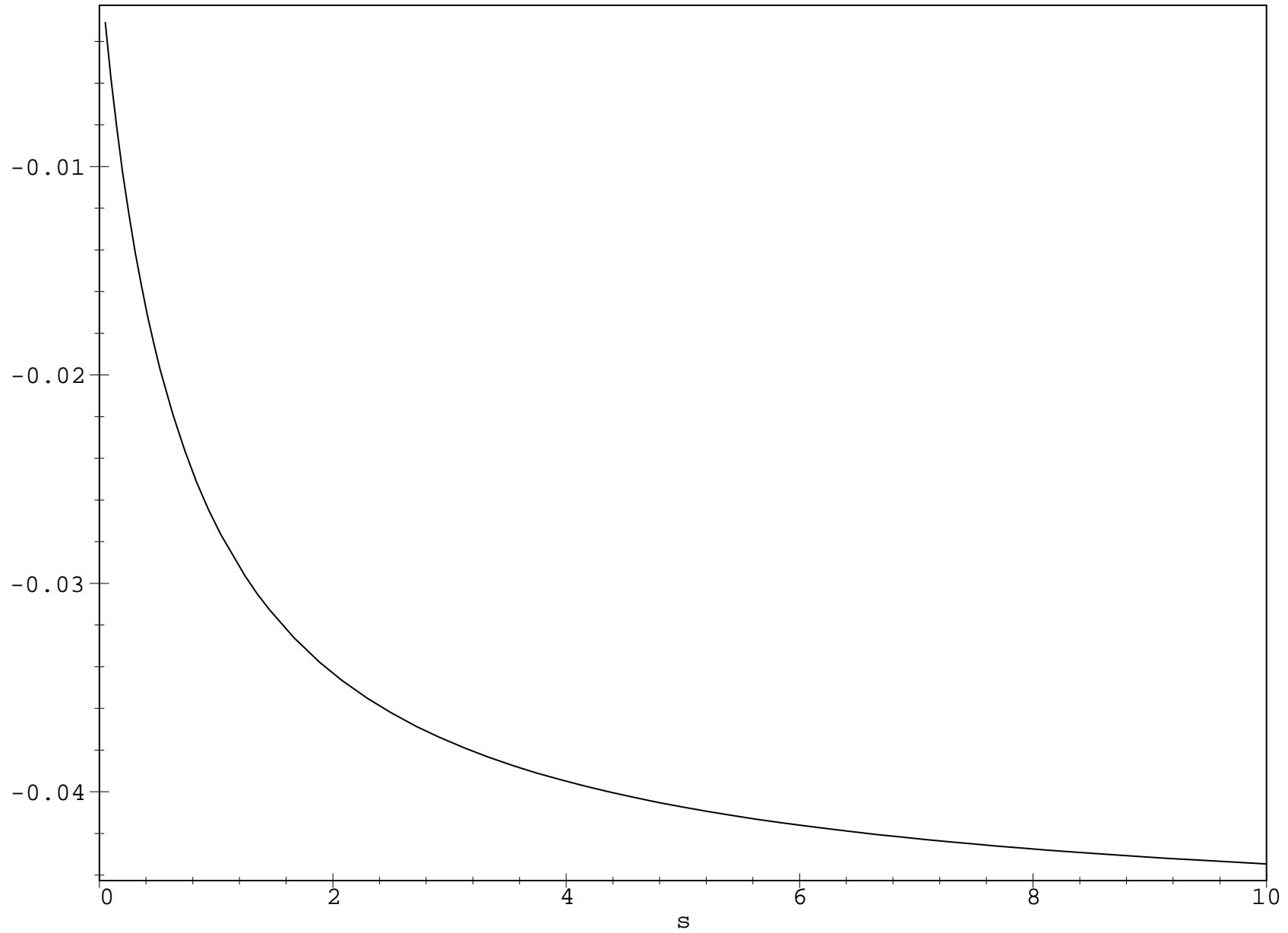
Fig. 14. Rayleigh reduction factor for radiation pressure ($s = 100$) as a function of grain eccentricity. The solid line corresponds to the temperature ratio 100, the dotted line corresponds to 10 and the dashed line corresponds to 1.1.



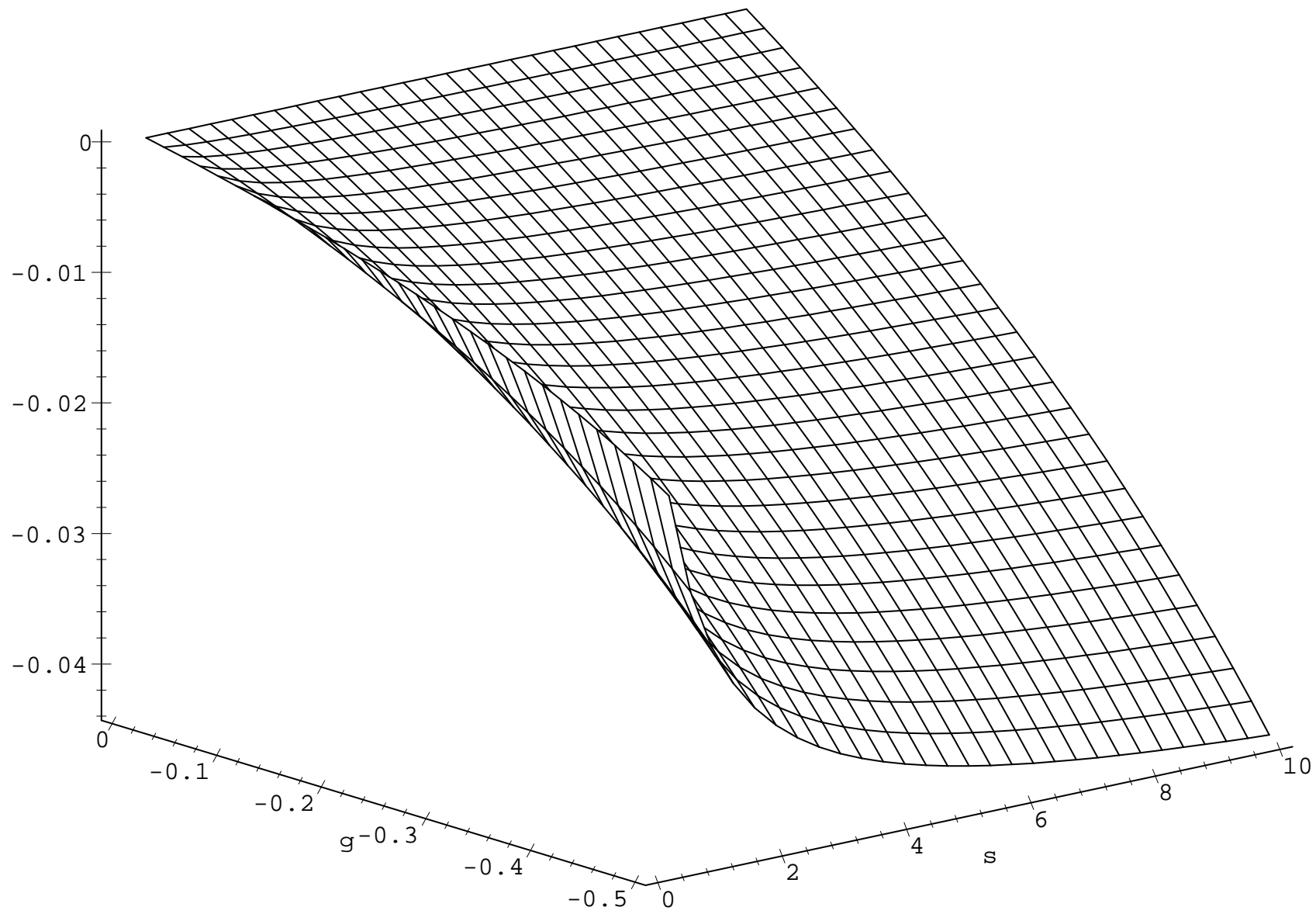
measure of alignment, R , for $s=-0.5$



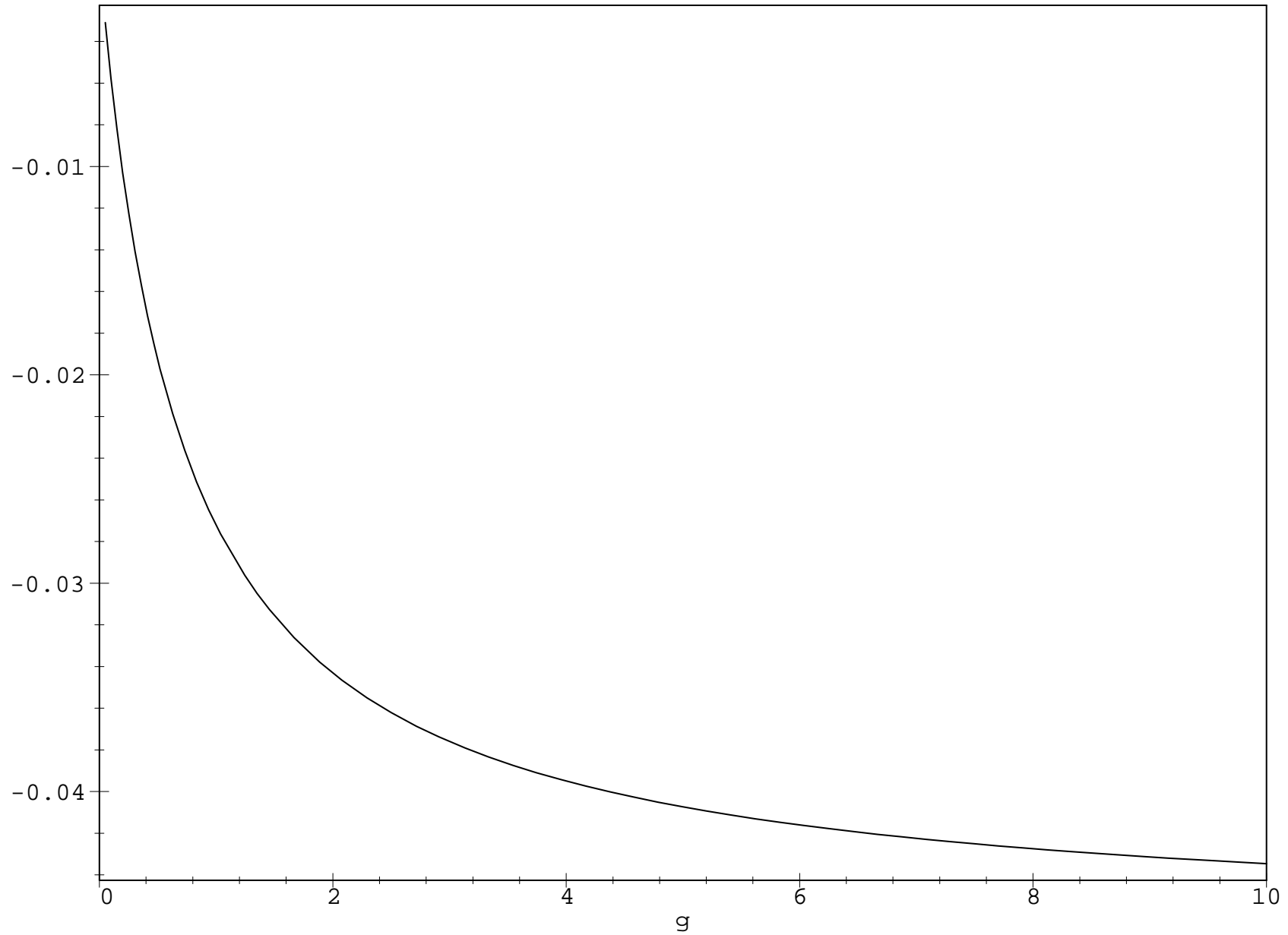
measure of alignment, R , for $g=-0.5$



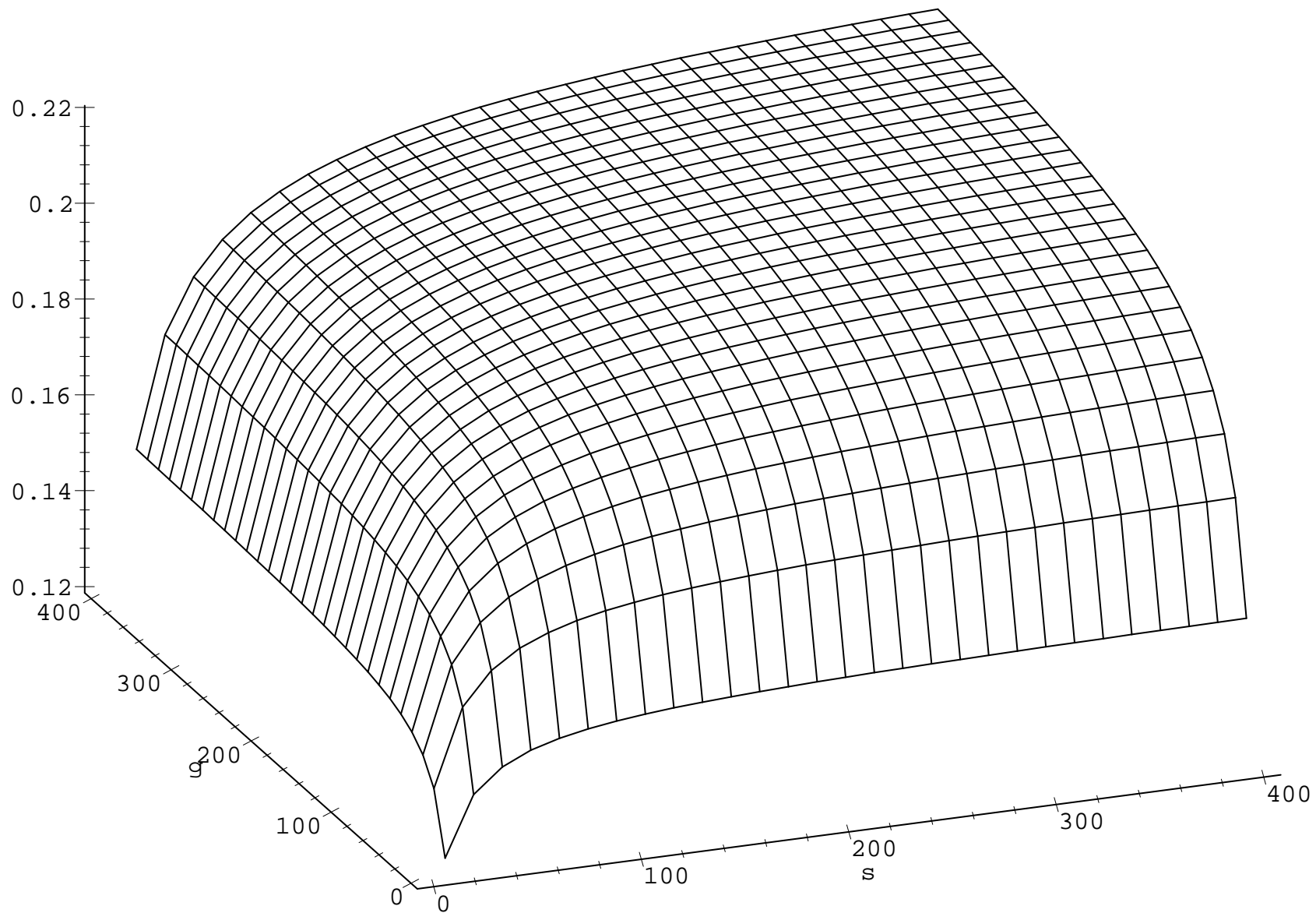
measure of alignment, R



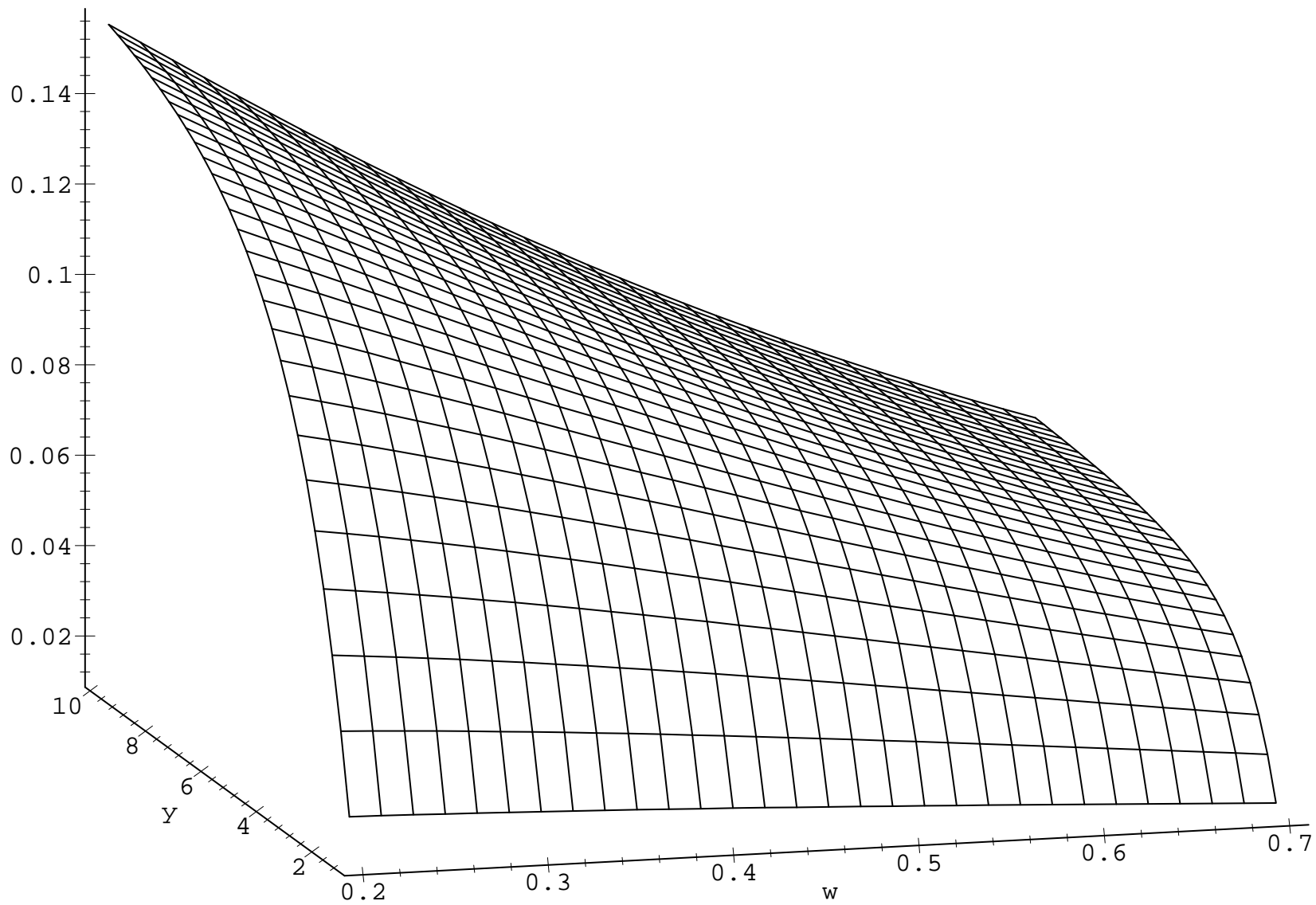
measure of alignment, R , for $s=-0.5$



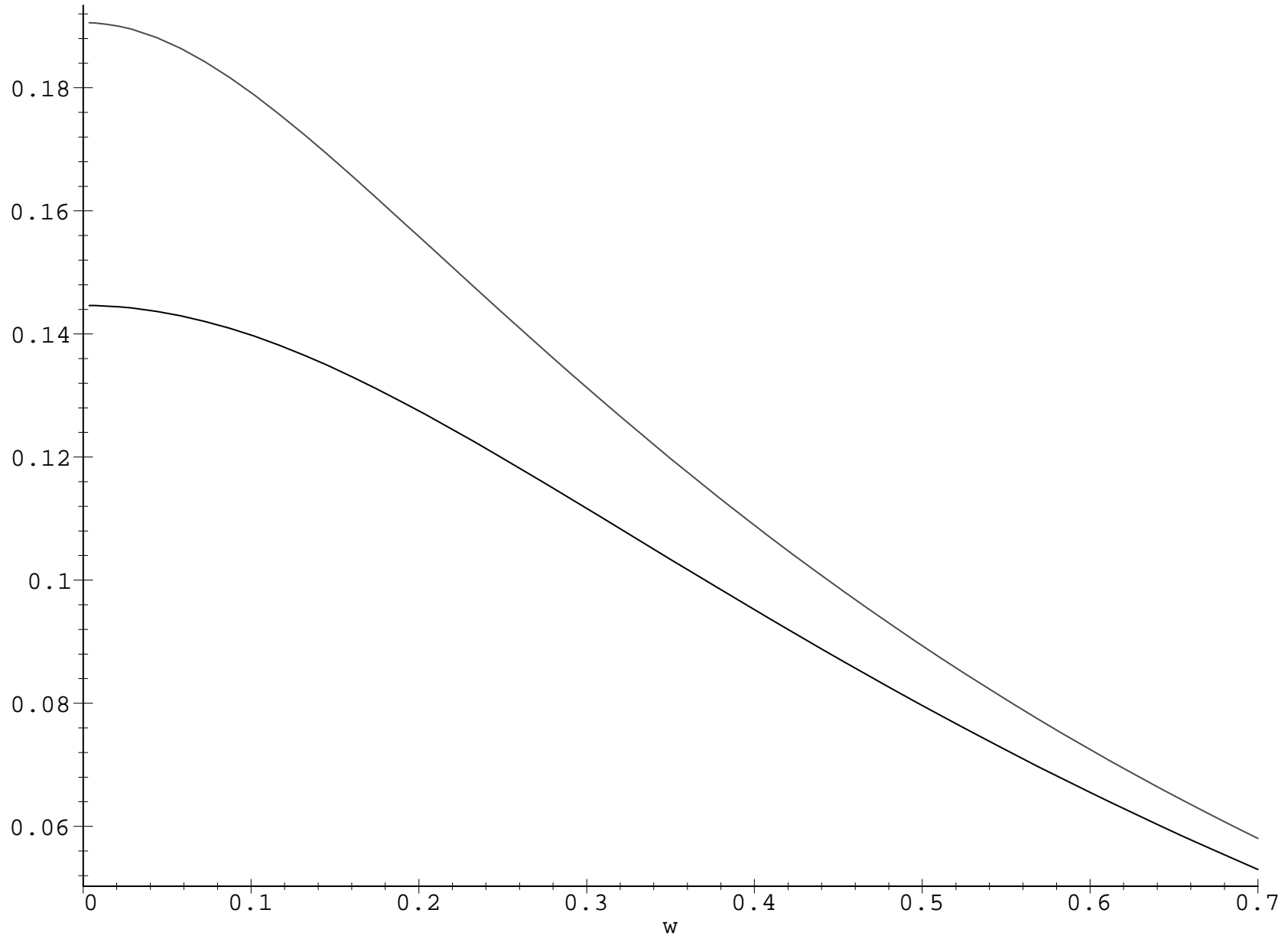
measure of alignment, R



measure of alignment, R



measure of alignment, R , for $y=5$ and $y=10$



measure of alignment, R

